

Article

Size-Dependent Buckling Analysis of Microbeams by an Analytical Solution and Isogeometric Analysis

Shuohui Yin ^{1,*}, Zhibing Xiao ¹, Gongye Zhang ^{2,*} , Jingang Liu ^{1,3} and Shuitao Gu ⁴ ¹ School of Mechanical Engineering and Mechanics, Xiangtan University, Xiangtan 411100, China² Jiangsu Key Laboratory of Engineering Mechanics, School of Civil Engineering, Southeast University, Nanjing 210096, China³ Xiangtan National Applied Mathematics Center, Xiangtan 411105, China⁴ School of Civil Engineering, Chongqing University, Chongqing 400044, China

* Correspondence: yinsh2016@163.com (S.Y.); gyzhang@seu.edu.cn (G.Z.)

Abstract: This paper proposes an analytical solution and isogeometric analysis numerical approach for buckling analysis of size-dependent beams based on a reformulated strain gradient elasticity theory (RSGET). The superiority of this method is that it has only one material parameter for couple stress and another material parameter for strain gradient effects. Using the RSGET and the principle of minimum potential energy, both non-classical Euler–Bernoulli and Timoshenko beam buckling models are developed. Moreover, the obtained governing equations are solved by an exact solution and isogeometric analysis approach, which conforms to the requirements of higher continuity in gradient elasticity theory. Numerical results are compared with exact solutions to reveal the accuracy of the current isogeometric analysis approach. The influences of length–scale parameter, length-to-thickness ratio, beam thickness and boundary conditions are investigated. Moreover, the difference between the buckling responses obtained by the Timoshenko and Euler–Bernoulli theories shows that the Euler–Bernoulli theory is suitable for slender beams.



Citation: Yin, S.; Xiao, Z.; Zhang, G.; Liu, J.; Gu, S. Size-Dependent Buckling Analysis of Microbeams by an Analytical Solution and Isogeometric Analysis. *Crystals* **2022**, *12*, 1282. <https://doi.org/10.3390/cryst12091282>

Academic Editor: Abdolhamid Akbarzadeh Shafaroudi

Received: 17 August 2022

Accepted: 3 September 2022

Published: 9 September 2022

Publisher's Note: MDPI stays neutral with regard to jurisdictional claims in published maps and institutional affiliations.



Copyright: © 2022 by the authors. Licensee MDPI, Basel, Switzerland. This article is an open access article distributed under the terms and conditions of the Creative Commons Attribution (CC BY) license (<https://creativecommons.org/licenses/by/4.0/>).

Keywords: buckling; size effect; microbeams; isogeometric analysis; strain gradient theory

1. Introduction

In the micro-/nano-electromechanical systems (M/NEMS) [1,2], micro/nanobeam structures are extensively used as actuators, atomic force microscopes [1,3], etc., due to the small size feature of micro/nanostructures; microstructure effects have been reported in some experiments [4,5]. On the other hand, the buckling instability problem observed in micro/nanobeams may happen when subjected to high compressive stress [6,7]. However, it is difficult to predict the size-dependent deformation behaviors in micro-scale structures using classical continuum theories as there is a lack of microstructure-scale parameters to consider the microstructure effects. Therefore, numerous higher-order continuum theories, including strain gradient theories [8,9], non-local elasticity theory [10,11], micropolar theory [12] and couple-stress theory, [13–15] which contain additional material parameters, have been developed to describe the microstructure effect.

Strain gradient elasticity theory was first presented by Mindlin [8], considering an isotropic elastic material with 16 intrinsic material parameters. The strain energy density function of this theory can be presented with three typical forms [9,16] and functions of the infinitesimal strain. Based on Fleck and Hutchinson's work [17], Lam et al. [4] reduced the material parameters in strain gradient theory to three, which is also known as modified strain gradient theory (MSGT). Since then, numerous non-classical beam models have been developed based on MSGT. By using MSGT, Kong et al. [18] presented a non-classical Euler–Bernoulli beam theory, and Wang et al. [19] established a non-classical Timoshenko beam theory. Akgöz et al. [20,21] applied the Euler–Bernoulli microbeam theory to study buckling and bending size-dependent behavior under various boundary conditions. Furthermore,

Akgöz and Civalek [22] and Ansari et al. [23] extended it to the functionally graded (FG) microbeams problem. As for non-local elasticity theory, lots of studies investigated the size-dependent effects on mechanical behavior using Eringen's non-local elasticity theory [10,11]. Reddy [24] applied non-local elasticity theory to study the mechanical response of microstructure beams. Barretta et al. [25] presented a consistent variational formulation to deal with the improper boundary conditions problem in non-local strain gradient beam formulation. After, Barretta et al. [26] unified Lam's strain gradient [4] and Eringen's non-local [10,11] theory through a variational formulation. The non-local strain gradient Timoshenko theory [26] is also used to calculate the Young modulus of carbon nanotubes (CNTs) [27]. Thang et al. [28] applied non-local strain gradient theory to study the mechanical response of bi-directional functionally graded (BDFG) nanobeams. By combining non-local strain gradient theory with a quasi-3D beam theory, Jalaei et al. [29] studied the viscoelastic transient behavior of magnetically imperfect FG nanobeams. Moreover, a simplified strain gradient elasticity theory (SSGET) [30,31] (known as dipolar gradient theory [32]) with only one material length scale parameter for the strain gradient effect was proposed by Altan and Aifantis [33]. Based on the SSGET, Hong et al. [34] extended it to the Kirchhoff microrods problem. According to the SSGET, Liang et al. [35] proposed a Euler–Bernoulli microbeam theory.

The couple-stress theory is also an important high-order continuum theory. It is worth noting that the classical couple-stress elasticity theory with four material-scale parameters proposed by Mindlin [14]. Afterwards, Yang et al. [36] developed a modified couple-stress theory (MCST) with only one scale parameter. Based on modified couple-stress theory and non-local elasticity theory, a non-local couple-stress theory was developed by Ebrahimi et al. [37] for functionally graded (FG) nanobeams. On the other hand, the modified strain gradient theory [4] can be further simplified to the MCST [36,38,39] by neglecting the symmetric second gradient of displacement. Based on MCST, a large amount of non-classical microbeam models have been developed for Euler–Bernoulli [39,40], Timoshenko [41,42] and Reddy–Levinson beams [43,44]. Recently, Hong et al. [45,46] extended the MCST to the static, free vibration and wave propagation problems of the magneto-electro-elastic (MEE) FG microbeam and MEE FG porous microbeam.

However, strain gradient elasticity theory or couple-stress theory only considers the effect of strain gradient or couple stress. In order to contain both effects and with fewer material parameters, Zhang and Gao [47] derived a reformulated strain gradient elasticity theory (RSGET) with one material constant for each. A new Euler–Bernoulli microbeam model was developed using the RSGET [47] and extended for mechanical behavior of FG microbeams [48]. On the other hand, as the higher continuity requirements of higher-order continuum theories, the traditional finite element method needs special technology to establish the strain gradient [49–52]. Therefore, a higher-order numerical approach combined with higher-order continuum theories must be developed for size-dependent analysis of microstructures.

Isogeometric analysis (IGA) based on splines basis functions is a higher-order computational approach proposed by Hughes et al. [53]. Due to the higher-order approximation, it has been extensively applied to study the size effect of micro/nanostructures. Nguyen et al. [54] investigated size effects on the bending, vibration and buckling behaviors of FG nanoplates by utilizing IGA with non-local elasticity theory. Ansari and Norouzzadeh [55] applied IGA to study the buckling behavior of FG nanoplates with the non-local and surface effects. Phung-Van et al. [56] studied the nonlinear behaviors of FG nanoplates by IGA and provided a computational optimization [57,58] for functionally graded sandwich nanoplates. Nguyen et al. [59] combined an isogeometric approach with the MCST for functionally graded microplates problems. Liu et al. [60] developed an isogeometric analysis approach based on MCST and surface energy for thin nanoplates. Using MCST and isogeometric analysis, Thanh et al. [61] and Farzam et al. [62] studied the mechanical behavior of FG carbon-nanotube-reinforced composite plates. Thai et al. [63] uses isogeometric analysis approach and modified strain gradient theory [4] to investigate

the static, vibration and buckling responses of FG microplates. The non-classical Timoshenko and Euler–Bernoulli isogeometric analysis approaches, based on the MCST and the surface elasticity theory, are presented by Yin et al. [64,65]. By using an isogeometric analysis approach and RSGET, Yin et al. [66,67] investigated the microstructure effect on the mechanical response of microbeam. Phung-Van et al. [68] use isogeometric analysis with a non-local strain gradient theory to investigate the porosity of the metal foam nanoscale plates. However, based on literature review, an isogeometric analysis approach for buckling analysis of microbeam considering both couple stress and strain gradient effects has not been developed yet.

The main aim of this work is to introduce a non-classical microbeam model for buckling analysis which includes couple stress and strain gradient effects by a reformulated strain gradient elasticity theory. The paper is structured as follows. Section 2 presents the reformulated strain gradient elasticity theory, the non-classical Euler–Bernoulli beam theory, and the Timoshenko beam theory. Section 3 describes the analytical solution of non-classical Euler–Bernoulli and Timoshenko beam formulations. Section 4 focuses on NURBS-based isogeometric analysis discretization equations. The numerical examples are presented in Section 5 and the isogeometric analysis results are compared with analytical solutions. Finally, the conclusions and summary are presented in Section 6.

2. Basic Formulation

2.1. A Brief of Reformulated Strain Gradient Elasticity Theory

In this study, a reformulated strain gradient elasticity theory (RSGET), originally proposed by Zhang and Gao [47], is adopted. The superiority of this theory is that it can simultaneously incorporate the couple-stress effects and strain gradient effects with only one scale parameter for each. Considering an isotropic linear elastic body, the strain energy U from RSGET [47] is defined by

$$U = \int_{\Omega} (\sigma_{ij}\varepsilon_{ij} + \tau_{ijk}^s \eta_{ijk}^s + m_{ij}\chi_{ij}) dV \quad (1)$$

where the Cauchy stress tensor, σ_{ij} , the symmetric part of the double-stress tensor, τ_{ijk}^s , and the couple-stress tensor, m_{ij} , are given by

$$\sigma_{ij} = \lambda \varepsilon_{kk} \delta_{ij} + 2\mu \varepsilon_{ij} \quad (2)$$

$$\tau_{ijk}^s = 2l_s^2 \mu \eta_{ijk}^s \quad (3)$$

$$m_{ij} = 2l_m^2 \mu \chi_{ij} \quad (4)$$

in which the Lamé constants λ and μ are defined as

$$\lambda = \frac{Ev}{(1+v)(1-2v)}, \quad \mu = \frac{E}{2(1+v)} \quad (5)$$

where δ_{ij} refers to the Kronecker delta, l_s and l_m are the material length-scale parameter for the strain gradient effect and the couple-stress effect, respectively. E is Young's modulus and ν is Poisson's ratio. The strain tensor, ε_{ij} , the symmetric part of second-order displacement gradient tensor, η_{ijk}^s , and the curvature tensor, χ_{ij} , are, respectively, expressed by

$$\varepsilon_{ij} = \frac{1}{2}(u_{i,j} + u_{j,i}) \quad (6)$$

$$\eta_{ijk}^s = \frac{1}{3}(u_{i,jk} + u_{j,ki} + u_{k,ij}) \quad (7)$$

$$\chi_{ij} = \frac{1}{2}(\theta_{i,j} + \theta_{j,i}) \quad (8)$$

where u_i is the displacement and θ_i is the rotation vector, written as

$$\theta_i = \frac{1}{2}e_{ijk}u_{k,j} \tag{9}$$

with e_{ijk} as the replacement tensor.

Consider a microbeam under compression P as shown in Figure 1; the geometry parameters are width, b , thickness, h , and length, L , and the displacement field of any point on the cross-section of Timoshenko beam can be depicted as

$$u_1 = -z\varphi(x), u_2 = 0, u_3 = w(x) \tag{10}$$

in which u_i ($i = 1, 2, 3$) represents the displacement of any point (x, y, z) on the beam section; φ denotes the angle of rotation about the y -axis; w is the z -direction displacement on the x -axis. By setting $\varphi(x) = \partial w(x)/\partial x$ in above equations, the displacement field of Euler–Bernoulli (classical) beam can be derived.

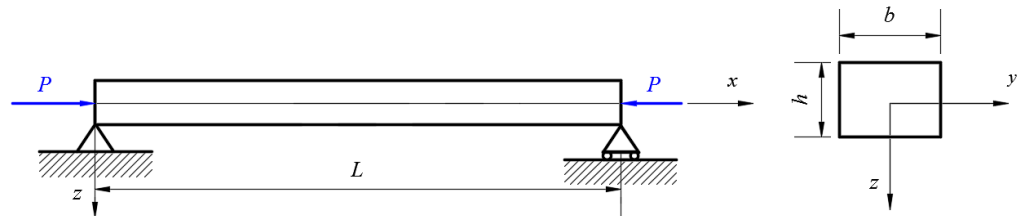


Figure 1. A schematic of a clamped simple-supported beam.

2.2. Buckling Analysis of Non-Classical Euler–Bernoulli Beam Theory

In Euler–Bernoulli beam, the displacement expression is obtained by setting $\varphi(x, t) = \partial w(x, t)/\partial x$ in Equation (10). By substituting the displacement Equation (10) into Equations (6)–(9), one yields the components of a non-zero strain, the symmetric part of a second-order displacement gradient, the curvature and the rotation vector as follows:

$$\varepsilon_{xx} = -z \frac{\partial^2 w}{\partial x^2} \tag{11}$$

$$\eta_{xxx}^s = -z \frac{\partial^3 w}{\partial x^3}, \eta_{xxz}^s = -\frac{1}{3} \frac{\partial^2 w}{\partial x^2} \tag{12}$$

$$\chi_{xy} = -\frac{1}{2} \frac{\partial^2 w}{\partial x^2} \tag{13}$$

$$\theta_y = -\frac{\partial w}{\partial x} \tag{14}$$

As η_{xxx}^s is higher order than the displacement gradient η_{xxz}^s [69,70], hence, the rest of the formulation ignored the effect of η_{xxx}^s .

As for a large aspect ratio, the slender beam assumption is adopted and the Lamé constants $(\lambda + 2\mu)$ is simplified to Young’s modulus E . By using Equations (11)–(14) and (2)–(4), the non-zero Cauchy stress and the symmetric parts of the double stress and couple stress are written as

$$\sigma_{xx} = -Ez \frac{\partial^2 w}{\partial x^2}, \sigma_{yy} = \sigma_{zz} = -Ez \frac{\partial^2 w}{\partial x^2} \tag{15}$$

$$\tau_{xxz}^s = -\frac{2}{3}l_s^2\mu \frac{\partial^2 w}{\partial x^2} \tag{16}$$

$$m_{xy} = -\mu l_m^2 \frac{\partial^2 w}{\partial x^2} \tag{17}$$

Based on the variational principle, the total strain energy derived by substituting Equations (15)–(17) and (11)–(13) into Equation (1), is as follows:

$$\begin{aligned} \delta U &= \int_0^L \left(-M_x \delta \frac{\partial^2 w}{\partial x^2} - Y_x \delta \frac{\partial^2 w}{\partial x^2} - Q_x \delta \frac{\partial^2 w}{\partial x^2} \right) dx \\ &= -\int_0^L \left(\frac{\partial^2 M_x}{\partial x^2} + \frac{\partial^2 Y_x}{\partial x^2} + \frac{\partial^2 Q_x}{\partial x^2} \right) \delta w dx + \left[\left(\frac{\partial Y_x}{\partial x} + \frac{\partial M_x}{\partial x} + \frac{\partial Q_x}{\partial x} \right) \delta w \right. \\ &\quad \left. + (-M_x - Y_x - Q_x) \delta \frac{\partial w}{\partial x} \right] \Big|_0^L \end{aligned} \tag{18}$$

where

$$\begin{aligned} M_x &= \int_A \sigma_{xx} z dA = -EI \frac{\partial^2 w}{\partial x^2}, \\ Y_x &= \int_A m_{xy} dA = -\mu l_m^2 \frac{\partial^2 w}{\partial x^2}, \\ Q_x &= \int_A \tau_{xxz}^s dA = -\frac{2}{3} l_s^2 \mu A \frac{\partial^2 w}{\partial x^2} \end{aligned} \tag{19}$$

Equation (19) is the stress results of the current Euler–Bernoulli beam model, where A and I are, respectively, the area and the second moment of cross-sectional given by

$$A = bh, \quad I = \int_A z^2 dA = \frac{1}{12} bh^3 \tag{20}$$

For buckling analysis, the virtual work done by the transverse load q and the in-plane axial compressive force, P , on the current beam model can be given as [39,71]

$$\delta W = \int_0^L (q \delta w + c \delta \theta_y + P \frac{\partial w}{\partial x} \delta \frac{\partial w}{\partial x}) dx + \left[\bar{V} \delta w - \bar{H} \delta \left(\frac{\partial w}{\partial x} \right) \right] \Big|_0^L \tag{21}$$

in which q denotes the body force per unit length in z -direction; c represents the body couple per unit length in y -direction; θ_y is given from Equation (14); \bar{V} and \bar{H} are the transverse shear force and the high-order bending moment, respectively.

The first variation of the total potential energy can be obtained as [38,72]

$$\delta \Pi_G = \delta U - \delta W \tag{22}$$

Using Equations (18) and (21) in Equation (22), and applying the principle of total minimum potential energy, i.e., $\delta \Pi_G = 0$, and the fundamental lemma of the calculus of variations [73] will be obtained in the equilibrium equation of the Euler–Bernoulli beam as follows:

$$-\frac{\partial^2 M_x}{\partial x^2} - \frac{\partial^2 Y_x}{\partial x^2} - \frac{\partial^2 Q_x}{\partial x^2} + P \frac{\partial^2 w}{\partial x^2} - \frac{\partial c}{\partial x} - q = 0 \tag{23}$$

where the boundary conditions are

$$\begin{aligned} -M_x - Y_x - Q_x + \bar{H} = 0 \quad \text{or} \quad \frac{\partial w}{\partial x} = \frac{\partial \bar{w}}{\partial x} \quad \text{at} \quad x = 0, L \\ \frac{\partial Y_x}{\partial x} + \frac{\partial M_x}{\partial x} + \frac{\partial Q_x}{\partial x} - P \frac{\partial w}{\partial x} + c - \bar{V} = 0 \quad \text{or} \quad w = \bar{w} \quad \text{at} \quad x = 0, L \end{aligned} \tag{24}$$

Substituting Equation (19) into Equation (23) and considering $q = c = 0$, we then obtained the equilibrium equation of the Euler–Bernoulli beam in regard to displacement, w , as follows:

$$\left(EI + \mu l_m^2 A \right) \frac{\partial^4 w}{\partial x^4} + \frac{2}{3} l_s^2 \mu A \frac{\partial^4 w}{\partial x^4} + P \frac{\partial^2 w}{\partial x^2} = 0 \tag{25}$$

It can be observed from Equation (25) that the present Euler–Bernoulli beam formulation includes two material–scale parameters (i.e., l_s and l_m) for describing the microstructure-dependent elastic properties.

When $l_s = 0$, Equation (25) degenerates to the governing equation of the non-classical Euler–Bernoulli beam model, derived by the modified couple-stress theory [39], as follows:

$$\left(EI + \mu l_m^2 A \right) \frac{\partial^4 w}{\partial x^4} + P \frac{\partial^2 w}{\partial x^2} = 0 \tag{26}$$

When $l_s = l_m = 0$, the governing equation from Equation (25) will degenerate to the classical Euler–Bernoulli beam formulation (classical), which is given as

$$EI \frac{\partial^4 w}{\partial x^4} + P \frac{\partial^2 w}{\partial x^2} = 0 \quad (27)$$

2.3. Buckling Analysis of Non-Classical Timoshenko Beam Theory

For Timoshenko microbeams, the derivation is the same as above; using Equation (10) and Equations (6)–(9), the non-zero strain tensor, second-order displacement gradient tensor, curvature tensor and rotation vector are, respectively, derived as

$$\varepsilon_{xx} = -z \frac{\partial \varphi}{\partial x}, \quad \varepsilon_{xz} = \frac{1}{2} \left(\frac{\partial w}{\partial x} - \varphi \right) \quad (28)$$

$$\eta_{xxx}^s = -z \frac{\partial^2 \varphi}{\partial x^2}, \quad \eta_{xxz}^s = \frac{1}{3} \frac{\partial^2 w}{\partial x^2} - \frac{2}{3} \frac{\partial \varphi}{\partial x} \quad (29)$$

$$\chi_{xy} = -\frac{1}{4} \left(\frac{\partial^2 w}{\partial x^2} + \frac{\partial \varphi}{\partial x} \right) \quad (30)$$

$$\theta_y = -\frac{1}{2} \left(\frac{\partial w}{\partial x} + \varphi \right) \quad (31)$$

It is important to note that, the higher-order displacement gradient η_{xxx}^s is also neglected in the Timoshenko formulation.

By using Equations (28)–(31) and (2)–(4), the non-zero Cauchy stress, symmetric part of double stress and couple stress are written as follows:

$$\begin{aligned} \sigma_{xx} &= -\frac{E(1-\nu)}{(1+\nu)(1-2\nu)} z \frac{\partial \varphi}{\partial x} \\ \sigma_{yy} = \sigma_{zz} &= -\frac{E\nu}{(1+\nu)(1-2\nu)} z \frac{\partial \varphi}{\partial x} \\ \sigma_{xz} &= \frac{E}{2(1+\nu)} \left(\frac{\partial w}{\partial x} - \varphi \right) \end{aligned} \quad (32)$$

$$\tau_{xxz}^s = 2l_s^2 \mu \left(\frac{1}{3} \frac{\partial^2 w}{\partial x^2} - \frac{2}{3} \frac{\partial \varphi}{\partial x} \right) \quad (33)$$

$$m_{xy} = -\frac{1}{2} \mu l_m^2 \left(\frac{\partial^2 w}{\partial x^2} + \frac{\partial \varphi}{\partial x} \right) \quad (34)$$

Substituting Equations (28)–(31) and Equations (32)–(34) into Equation (1), we obtain the first variation of the total strain energy as

$$\begin{aligned} \delta U &= \int_0^L \left[-M_x \delta \frac{\partial \varphi}{\partial x} + R_x \delta \left(\frac{\partial w}{\partial x} - \varphi \right) - \frac{1}{2} Y_x \delta \left(\frac{\partial^2 w}{\partial x^2} + \frac{\partial \varphi}{\partial x} \right) + Q_x \delta \left(\frac{\partial^2 w}{\partial x^2} - 2 \frac{\partial \varphi}{\partial x} \right) \right] dx \\ &= \int_0^L \left(\frac{\partial M_x}{\partial x} - R_x + \frac{1}{2} \frac{\partial Y_x}{\partial x} + 2 \frac{\partial Q_x}{\partial x} \right) \delta \varphi dx + \int_0^L \left(-\frac{\partial R_x}{\partial x} - \frac{1}{2} \frac{\partial^2 Y_x}{\partial x^2} + \frac{\partial^2 Q_x}{\partial x^2} \right) \delta w dx \\ &+ \left[\left(-\frac{1}{2} Y_x - M_x - 2Q_x \right) \delta \varphi + \left(R_x + \frac{1}{2} \frac{\partial Y_x}{\partial x} - \frac{\partial Q_x}{\partial x} \right) \delta w + \left(Q_x - \frac{1}{2} Y_x \right) \delta \frac{\partial w}{\partial x} \right] \Big|_0^L \end{aligned} \quad (35)$$

in which

$$\begin{aligned} M_x &= \int_A \sigma_{xx} z dA = -\frac{E(1-\nu)I}{(1+\nu)(1-2\nu)} \frac{\partial \varphi}{\partial x}, \quad R_x = \int_A \sigma_{xz} dA = K_S \mu A \left(\frac{\partial w}{\partial x} - \varphi \right), \\ Y_x &= \int_A m_{xy} dA = -\frac{1}{2} \mu l_m^2 A \left(\frac{\partial^2 w}{\partial x^2} + \frac{\partial \varphi}{\partial x} \right), \quad Q_x = \int_A \tau_{xxz}^s dA = 2l_s^2 \mu A \left(\frac{1}{3} \frac{\partial^2 w}{\partial x^2} - \frac{2}{3} \frac{\partial \varphi}{\partial x} \right) \end{aligned} \quad (36)$$

Equation (36) is the stress result of the current Timoshenko beam model. The shear constant is given as $K_S = (5 + 5\nu)/(6 + 5\nu)$.

For buckling analysis, the virtual work done by external forces can be given by [41,71]

$$\delta W = \int_0^L (q\delta w + c\delta\theta_y + P\frac{\partial w}{\partial x}\delta\frac{\partial w}{\partial x})dx + \left[\bar{V}\delta w - \bar{M}\delta\varphi - \bar{H}\delta\left(\frac{\partial w}{\partial x}\right) \right]_0^L \quad (37)$$

where θ_y is given from Equation (31) and \bar{M} is the bending moment.

According to the principle of total minimum potential energy, substituting Equations (35) and (37) into Equation (22) and employing the principle of the calculus of variations [73], the equilibrium equations of the Timoshenko beam are achieved as

$$\begin{aligned} & \frac{E(1-\nu)I}{(1+\nu)(1-2\nu)}\frac{\partial^2\varphi}{\partial x^2} + K_s\mu A\left(\frac{\partial w}{\partial x} - \varphi\right) \\ & + \frac{1}{4}\mu l_m^2 A\left(\frac{\partial^3 w}{\partial x^3} + \frac{\partial^2\varphi}{\partial x^2}\right) - 4l_s^2\mu A\left(\frac{1}{3}\frac{\partial^3 w}{\partial x^3} - \frac{2}{3}\frac{\partial^2\varphi}{\partial x^2}\right) - \frac{1}{2}c = 0 \\ & - K_s\mu A\left(\frac{\partial^2 w}{\partial x^2} - \frac{\partial\varphi}{\partial x}\right) + \frac{1}{4}\mu l_m^2 A\left(\frac{\partial^4 w}{\partial x^4} + \frac{\partial^3\varphi}{\partial x^3}\right) \\ & + 2l_s^2\mu A\left(\frac{1}{3}\frac{\partial^4 w}{\partial x^4} - \frac{2}{3}\frac{\partial^3\varphi}{\partial x^3}\right) + P\frac{\partial^2 w}{\partial x^2} - q - \frac{1}{2}c = 0 \end{aligned} \quad (38)$$

and the boundary conditions are obtained as

$$\begin{aligned} R_x + \frac{1}{2}\frac{\partial Y_x}{\partial x} - \frac{\partial Q_x}{\partial x} - \bar{V} - P\frac{\partial w}{\partial x} + \frac{1}{2}c &= 0 \quad orw = \bar{w} \quad atx = 0, L \\ \frac{1}{2}Y_x + M_x + 2Q_x + \bar{M} &= 0 \quad or\varphi = \bar{\varphi} \quad atx = 0, L \\ Q_x - \frac{1}{2}Y + \bar{H} &= 0 \quad or\frac{\partial w}{\partial x} = \frac{\partial\bar{w}}{\partial x} \quad atx = 0, L \end{aligned} \quad (39)$$

It also can be seen from Equation (38) that two material-scale parameters (i.e., l_s and l_m) for describing the microstructure dependent elastic properties are contained in the present Timoshenko beam formulation.

When $l_s = 0$ and $q = c = 0$, Equation (38) degenerates to the governing equations of non-classical Timoshenko beam model derived from the modified couple-stress model [41], as follows:

$$\begin{aligned} & \frac{E(1-\nu)I}{(1+\nu)(1-2\nu)}\frac{\partial^2\varphi}{\partial x^2} + K_s\mu A\left(\frac{\partial w}{\partial x} - \varphi\right) + \frac{1}{4}\mu l_m^2 A\left(\frac{\partial^3 w}{\partial x^3} + \frac{\partial^2\varphi}{\partial x^2}\right) = 0 \\ & - K_s\mu A\left(\frac{\partial^2 w}{\partial x^2} - \frac{\partial\varphi}{\partial x}\right) + \frac{1}{4}\mu l_m^2 A\left(\frac{\partial^4 w}{\partial x^4} + \frac{\partial^3\varphi}{\partial x^3}\right) + P\frac{\partial^2 w}{\partial x^2} = 0 \end{aligned} \quad (40)$$

When $l_s = l_m = 0$ and $q = c = 0$, Equation (38) will degenerate to the classical Timoshenko beam model (classical) [41], which is given as follows:

$$\begin{aligned} & \frac{E(1-\nu)I}{(1+\nu)(1-2\nu)}\frac{\partial^2\varphi}{\partial x^2} + K_s\mu A\left(\frac{\partial w}{\partial x} - \varphi\right) = 0 \\ & - K_s\mu A\left(\frac{\partial^2 w}{\partial x^2} - \frac{\partial\varphi}{\partial x}\right) + P\frac{\partial^2 w}{\partial x^2} = 0 \end{aligned} \quad (41)$$

3. Analytical Solution

The critical buckling load of a simply supported microbeams as shown in Figure 1, are solved by analytical method with both Euler–Bernoulli beam theory (EBT) and Timoshenko beam theory (TBT) based on the reformulated strain gradient elasticity theory.

The Fourier series expansions are considered for $w(x)$ and $\varphi(x)$, given as follows

$$w(x) = \sum_{n=1}^{\infty} W_n \sin\left(\frac{n\pi x}{L}\right), \quad \varphi(x) = \sum_{n=1}^{\infty} \Phi_n \cos\left(\frac{n\pi x}{L}\right) \quad (42)$$

in which W_n and Φ_n are Fourier coefficients with respect to n . It shows that the boundary conditions in Equations (24) and (39) can be achieved by $w(x)$ and $\varphi(x)$ in Equation (42) for any W_n and Φ_n . It also should be noted that the $\varphi(x)$ should be ignored for Euler–Bernoulli beam.

3.1. Analytical Solution of Non-Classical Euler–Bernoulli Beam

In view of Equations (23) and (24), the simply supported boundary conditions of this Euler–Bernoulli beam can be described as

$$w|_{x=0} = w|_{x=L} = 0, EI \frac{\partial^2 w}{\partial x^2} + \mu A l_m^2 \frac{\partial^2 w}{\partial x^2} + \frac{2}{3} l_s^2 \mu A \frac{\partial^2 w}{\partial x^2} = 0 \quad \text{at } x = 0, L \quad (43)$$

Substituting Equation (42) into Equation (25), the critical buckling load P_{cr} of Euler–Bernoulli beam can be obtained as follows:

$$P_{cr} = \left(EI + \frac{2}{3} \mu A l_s^2 + \mu A l_m^2 \right) \left(\frac{\pi^2}{L^2} \right) \quad (44)$$

When $l_s = 0$, Equation (44) reduced to the formulation of non-classical Euler–Bernoulli beam derived from MCST [71], as follows:

$$P_{cr} = \left(EI + \mu A l_m^2 \right) \left(\frac{\pi^2}{L^2} \right) \quad (45)$$

When $l_s = l_m = 0$, Equation (44) degenerates to

$$P_{cr} = EI \left(\frac{\pi^2}{L^2} \right) \quad (46)$$

which is identical to the well-known critical buckling load given by the classical beam theory shown in Figure 1 from the mechanics of materials.

3.2. Analytical Solution of Non-Classical Timoshenko Beam

Using Equations (36) and (39), the simply supported boundary condition of Timoshenko beam can be rewritten as

$$\begin{aligned} w|_{x=0} = w|_{x=L} = 0 \\ 4l_s^2 \mu A \left(\frac{1}{3} \frac{\partial^2 w}{\partial x^2} - \frac{2}{3} \frac{\partial \varphi}{\partial x} \right) - \frac{E(1-\nu)I}{(1+\nu)(1-2\nu)} \frac{\partial \varphi}{\partial x} - \frac{1}{4} \mu l_m^2 A \left(\frac{\partial^2 w}{\partial x^2} + \frac{\partial \varphi}{\partial x} \right) = 0 \\ \frac{1}{4} \mu l_m^2 A \left(\frac{\partial^2 w}{\partial x^2} + \frac{\partial \varphi}{\partial x} \right) + 2l_s^2 \mu A \left(\frac{1}{3} \frac{\partial^2 w}{\partial x^2} - \frac{2}{3} \frac{\partial \varphi}{\partial x} \right) = 0 \end{aligned} \quad (47)$$

Substituting Equation (42) into Equation (38) results in

$$\begin{aligned} \left[\frac{1}{4} \mu l_m^2 A \left(\frac{n\pi}{L} \right)^3 - K_s \mu A \left(\frac{n\pi}{L} \right) - \frac{4}{3} \mu l_s^2 A \left(\frac{n\pi}{L} \right)^3 \right] W_n + \left[\frac{8}{3} \mu l_s^2 A \left(\frac{n\pi}{L} \right)^2 \right. \\ \left. + \frac{E(1-\nu)I}{(1+\nu)(1-2\nu)} \left(\frac{n\pi}{L} \right)^2 + K_s \mu A + \frac{1}{4} \mu l_m^2 A \left(\frac{n\pi}{L} \right)^2 \right] \Phi_n = 0 \\ \left[\frac{2}{3} \mu l_s^2 A \left(\frac{n\pi}{L} \right)^4 + \frac{1}{4} \mu l_m^2 A \left(\frac{n\pi}{L} \right)^4 + K_s \mu A \left(\frac{n\pi}{L} \right)^2 - P \left(\frac{n\pi}{L} \right)^2 \right] W_n \\ + \left[\frac{1}{4} \mu l_m^2 A \left(\frac{n\pi}{L} \right)^3 - K_s \mu A \left(\frac{n\pi}{L} \right) - \frac{4}{3} \mu l_s^2 A \left(\frac{n\pi}{L} \right)^3 \right] \Phi_n = Q_n \end{aligned} \quad (48)$$

Hence, the solution of critical value for the axial compressive load, P_{cr} , is acquired, as follows:

$$\begin{aligned} P_{cr} &= \frac{\mu A \left(\frac{2}{3} l_s^2 l_m^2 \mu A \left(\frac{\pi}{L} \right)^2 + C_1 + C_2 \right)}{\frac{8}{3} \mu l_s^2 A + \frac{E(1-\nu)I}{(1+\nu)(1-2\nu)} + K_s \mu A \left(\frac{L}{\pi} \right)^2 + \frac{1}{4} \mu l_m^2 A} \\ C_1 &= \left(\frac{2}{3} l_s^2 + l_m^2 \right) \mu A K_s \\ C_2 &= \left[\frac{2}{3} l_s^2 + \frac{1}{4} l_m^2 + K_s \left(\frac{L}{\pi} \right)^2 \right] \left(\frac{\pi}{L} \right)^2 \frac{EI(1-\nu)}{(1+\nu)(1-2\nu)} \end{aligned} \quad (49)$$

When $l_s = 0$, Equation (49) degenerates to formulation of the non-classical Timoshenko beam based on the MCST [71], as follows:

$$P_{cr} = \frac{\mu A \left[\frac{1}{4} l_m^2 + K_s \left(\frac{L}{\pi} \right)^2 \right] \left(\frac{\pi}{L} \right)^2 \frac{EI(1-\nu)}{(1+\nu)(1-2\nu)} + K_s \mu^2 A^2 l_m^2}{\frac{E(1-\nu)I}{(1+\nu)(1-\nu)} + K_s \mu A \left(\frac{L}{\pi} \right)^2 + \frac{1}{4} \mu l_m^2 A} \quad (50)$$

When $l_s = l_m = 0$, Equation (49) reduces to

$$P_{cr} = \frac{\mu A K_s \left(\frac{L}{\pi} \right)^2 \left(\frac{\pi}{L} \right)^2 \frac{EI(1-\nu)}{(1+\nu)(1-2\nu)}}{\frac{E(1-\nu)I}{(1+\nu)(1-\nu)} + K_s \mu A \left(\frac{L}{\pi} \right)^2} \quad (51)$$

which is the equation for the classical Timoshenko beam model.

4. Isogeometric Analysis

In this section, the isogeometric analysis approach is developed here for buckling analysis of microbeams based on the above non-classical Euler–Bernoulli and Timoshenko beam models.

4.1. NURBS Basis Functions

A one-dimensional non-uniform rational B-spline (NURBS) basis functions with a polynomial order, p , is constructed from a weight B-spline function as follows

$$R_{i,p}(\xi) = \frac{N_{i,p}(\xi)w_i}{\sum_{j=1}^n N_{j,p}(\xi)w_j} \quad (52)$$

in which w_i is the i^{th} weight and ξ is the parametric coordinate; n represents the number of NURBS basis functions, which also is the number of control points; the i^{th} B-splines basis function $N_{i,p}(\xi)$ with degree of p is defined as

$$N_{i,0}(\xi) = \begin{cases} 1 & \text{if } \xi_i \leq \xi \leq \xi_{i+1} \\ 0 & \text{otherwise} \end{cases} \quad \text{for } p = 0$$

$$N_{i,p}(\xi) = \frac{\xi - \xi_i}{\xi_{i+p} - \xi_i} N_{i,p-1}(\xi) + \frac{\xi_{i+p+1} - \xi}{\xi_{i+p+1} - \xi_{i+1}} N_{i+1,p-1}(\xi) \quad \text{for } p \geq 1 \quad (53)$$

The generalized midplane displacement of the beam are approximated by the above NURBS basis functions given as

$$\mathbf{u}^h = \sum_I^{NP} R_I \mathbf{u}_I \quad (54)$$

in which $NP = p + 1$ is the number of control points in each element; \mathbf{u}_I and R_I denote, respectively, the displacement vector and the NURBS basis function at control point I .

4.2. A NURBS-Based Non-Classical Euler–Bernoulli Beam Formulation

According to the above non-classical Euler–Bernoulli beam formulation, the generalized displacement only includes the deflection given as

$$\mathbf{u}_I = w_I \quad (55)$$

Substituting Equation (55) into Equations (11)–(13), we can derive the following:

$$\begin{aligned} \epsilon_{xx} &= -z \sum_{I=1}^{NP} B_I^1 u_I \\ \eta_{xxz}^s &= - \sum_{I=1}^{NP} B_I^1 u_I \\ \chi_{xy} &= - \sum_{I=1}^{NP} B_I^1 u_I \end{aligned} \tag{56}$$

with

$$B_I^1 = R_{I,xx} \tag{57}$$

For buckling analysis, the discretized equations of the buckling microbeam can be written as

$$[\mathbf{K} - P_{cr} \mathbf{K}_g] \mathbf{X} = 0 \tag{58}$$

where P_{cr} is the critical buckling load and \mathbf{X} is the eigenvector (deflection) at all control points. \mathbf{K} is the global stiffness given by

$$\mathbf{K} = \int_0^L (B_I^1)^T D_1 B_I^1 dx + \int_0^L (B_I^1)^T D_s B_I^1 dx + \int_0^L (B_I^1)^T D_m B_I^1 dx \tag{59}$$

with

$$\begin{aligned} D_1 &= \int_{-h/2}^{h/2} z^2 b E dz = \frac{bh^3}{12} E \\ D_s &= \int_{-h/2}^{h/2} 2z^2 b \mu l_s^2 dz = \frac{bh^3}{6} \mu l_s^2 \\ D_m &= \int_{-h/2}^{h/2} b \mu l_m^2 dz = bh \mu l_m^2 \end{aligned} \tag{60}$$

The geometrical stiffness matrix, \mathbf{K}_g , is given as

$$\mathbf{K}_g = \int_0^L (B_I^{Kg})^T P B_I^{Kg} dx \tag{61}$$

with

$$B_I^{Kg} = \frac{dR}{dx} \tag{62}$$

4.3. A NURBS-Based Non-Classical Timoshenko Beam Formulation

According to the above non-classical Timoshenko beam formulation, the generalized displacement of the microbeam includes deflection and angle of rotation, as follows:

$$u_I = [w_I \ \phi_I]^T \tag{63}$$

From Equations (11)–(13), the strain, curvature and displacement gradient are rewritten as the following matrix:

$$\begin{aligned} \epsilon_{xx} &= -z \frac{\partial \varphi}{\partial x} = \mathbf{C}_1 \boldsymbol{\epsilon}_1 \\ \epsilon_{xz} &= \frac{1}{2} \left(\frac{\partial w}{\partial x} - \varphi \right) = \mathbf{C}_2 \boldsymbol{\epsilon}_2 \\ \chi_{xy} &= -\frac{1}{4} \left(\frac{\partial^2 w}{\partial x^2} + \frac{\partial \varphi}{\partial x} \right) = \mathbf{C}_2 \boldsymbol{\chi} \\ \eta_{xxz}^s &= \frac{1}{3} \frac{\partial^2 w}{\partial x^2} - \frac{2}{3} \frac{\partial \varphi}{\partial x} = \mathbf{C}_2 \boldsymbol{\eta}_1 \end{aligned} \tag{64}$$

with

$$\boldsymbol{\epsilon}_1 = \begin{bmatrix} 0 \\ \frac{\partial \varphi}{\partial x} \end{bmatrix}, \boldsymbol{\epsilon}_2 = \begin{bmatrix} \frac{1}{2} \frac{\partial w}{\partial x} \\ -\frac{1}{2} \varphi \end{bmatrix}, \boldsymbol{\chi} = \begin{bmatrix} -\frac{1}{4} \frac{\partial^2 w}{\partial x^2} \\ -\frac{1}{4} \frac{\partial \varphi}{\partial x} \end{bmatrix}, \boldsymbol{\eta}_1 = \begin{bmatrix} \frac{1}{3} \frac{\partial^2 w}{\partial x^2} \\ -\frac{2}{3} \frac{\partial \varphi}{\partial x} \end{bmatrix} \tag{65}$$

Substituting Equation (63) into Equation (64), the strain matrix, curvature matrix and second-order displacement gradient matrix are obtained as follows:

$$\boldsymbol{\varepsilon}_1 = \sum_{I=1}^{NP} \mathbf{B}_I^1 \mathbf{u}_I, \quad \boldsymbol{\varepsilon}_2 = \sum_{I=1}^{NP} \mathbf{B}_I^2 \mathbf{u}_I, \quad \boldsymbol{\chi} = \sum_{I=1}^{NP} \mathbf{B}_I^m \mathbf{u}_I, \quad \boldsymbol{\eta}_1 = \sum_{I=1}^{NP} \mathbf{B}_I^{s1} \mathbf{u}_I \quad (66)$$

with

$$\mathbf{B}_I^1 = \begin{bmatrix} 0 & 0 \\ 0 & -\frac{dR_I}{dx} \end{bmatrix}, \quad \mathbf{B}_I^2 = \begin{bmatrix} \frac{1}{2} \frac{dR_I}{dx} & 0 \\ 0 & -\frac{1}{2} R_I \end{bmatrix},$$

$$\mathbf{B}_I^m = \begin{bmatrix} -\frac{1}{4} \frac{d^2 R_I}{dx^2} & 0 \\ 0 & -\frac{1}{4} \frac{dR_I}{dx} \end{bmatrix}, \quad \mathbf{B}_I^{s1} = \begin{bmatrix} \frac{1}{3} \frac{d^2 R_I}{dx^2} & 0 \\ 0 & -\frac{2}{3} \frac{dR_I}{dx} \end{bmatrix} \quad (67)$$

Considering the non-classical Timoshenko beam, the global stiffness \mathbf{K} in Equation (58) is given as follows:

$$\mathbf{K} = \int_0^L \begin{bmatrix} \mathbf{B}_I^1 \\ \mathbf{B}_I^2 \end{bmatrix}^T \begin{bmatrix} \mathbf{D}_1 & 0 \\ 0 & \mathbf{D}_2 \end{bmatrix} \begin{bmatrix} \mathbf{B}_I^1 \\ \mathbf{B}_I^2 \end{bmatrix} dx + \int_0^L (\mathbf{B}_I^{s1})^T \mathbf{D}_{s1} \mathbf{B}_I^{s1} dx + \int_0^L (\mathbf{B}_I^m)^T \mathbf{D}_m \mathbf{B}_I^m dx \quad (68)$$

with

$$\mathbf{D}_1 = \frac{E(1-\nu)}{(1+\nu)(1-2\nu)} \begin{bmatrix} 0 & 0 \\ 0 & \frac{bh^3}{12} \end{bmatrix}, \quad \mathbf{D}_2 = \frac{2EbhK_s}{1+\nu} \begin{bmatrix} 1 & 1 \\ 1 & 1 \end{bmatrix},$$

$$\mathbf{D}_{s1} = \frac{3EbhI_s^2}{1+\nu} \begin{bmatrix} 1 & 1 \\ 1 & 1 \end{bmatrix}, \quad \mathbf{D}_m = \frac{2EbhI_m^2}{1+\nu} \begin{bmatrix} 1 & 1 \\ 1 & 1 \end{bmatrix} \quad (69)$$

Additionally, the geometrical stiffness matrix, \mathbf{K}_g , can be written as

$$\mathbf{K}_g = \int_0^L (\mathbf{B}_I^G)^T \mathbf{P} \mathbf{B}_I^G dx \quad (70)$$

with

$$\mathbf{B}_I^G = \begin{bmatrix} \frac{dR}{dx} & 0 \\ 0 & 0 \end{bmatrix} \quad (71)$$

5. Numerical Examples

This section provides the results of exact and isogeometric analysis solutions of critical buckling of the microbeams for different material–scale parameters, length-to-thickness ratio, beam thickness and boundary conditions. The geometry and loading of microbeams (as shown in Figure 1) are given with $L = 20h$ and $b = 2h$, and the thickness is $h = 17.6 \mu\text{m}$. The material is taken to be epoxy, whose material length–scale parameter $l_m = 17.6 \mu\text{m}$ has been experimentally observed by Lam et al. [4]; $E = 1.44 \text{ GPa}$ and $\nu = 0.38$. In order to certify the proposed beam model and isogeometric analysis method, the non-dimensional critical buckling load, $P_{cr}L^2/EI$, acquired by isogeometric analysis based on Euler–Bernoulli and Timoshenko, without considering size effect, is compared with the exact solution [20,71] in Table 1. As can be observed in Table 1, the IGA results matched the exact solution [20,71] very well.

Table 1. Comparison of the critical buckling load obtained by IGA with exact solutions for the h-h boundary condition.

Theory	Method	Control Points	h (μm)				
			17.6	52.8	88	123.2	158.4
EBT	Analytical [20]		52.7809	14.6375	11.5861	10.7453	10.3994
	Analytical [71]		52.7809	14.6375	11.5861	10.7453	10.3994
	IGA	15	52.7813	14.6376	11.5861	10.7454	10.3994
	IGA	20	52.7810	14.6376	11.5861	10.7454	10.3994
	IGA	30	52.7809	14.6375	11.5861	10.7453	10.3994
TBT	Analytical [20]		60.3571	22.9608	19.9491	19.1188	18.7770
	Analytical [71]		60.3571	22.9608	19.9491	19.1188	18.7771
	IGA	15	60.3572	22.9609	19.9491	19.1188	18.7771
	IGA	20	60.3571	22.9608	19.9491	19.1188	18.7771
	IGA	30	60.3571	22.9608	19.9491	19.1188	18.7771

Figure 2 shows the variation of critical buckling loads obtained by analytical and isogeometric analysis (IGA) of EBT and TBT based on classical theory; Figure 2 also shows MCST and RSGET for simply supported beams with different length-to-thickness ratios. The geometries are $b = 2h$ and $h = 17.6 \mu\text{m}$, and the loading of microbeams is shown in Figure 1. The classical theory and MCST results can be obtained from RSGET by set $l_s = l_m = 0$ and $l_s = 0$, respectively. The material-scale parameter of RSGET is assumed as $l_s = 1.2l_m$. It is shown from the figure that the IGA results matched very well with the analytical solutions for both beam problems. Additionally, the critical buckling load predicted by RSGET and MCST is always higher than that obtained by classical model, which also explains the size-dependent behavior. It can also be observed that the critical buckling load decreases as the beam length increases, which is due to a decrease in microbeam stiffness as the beam length increases.

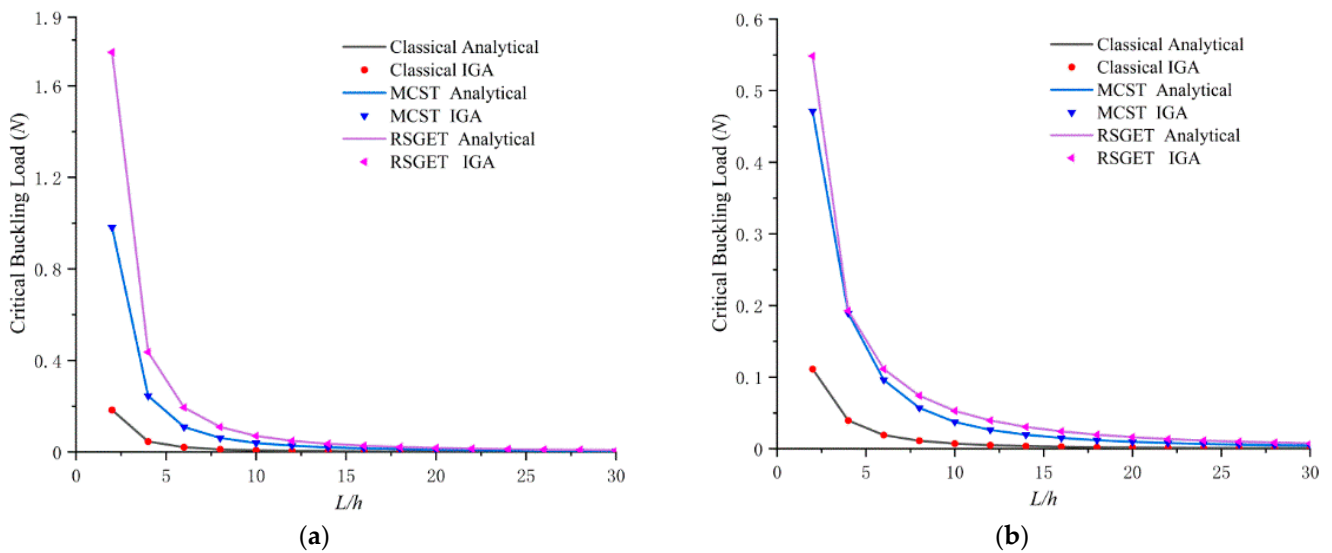


Figure 2. Critical buckling loads of the simply supported beam with different theories. (a) Euler–Bernoulli; (b) Timoshenko.

Considering the former example, Figure 3a,b shows the effect of different strain gradient length–scale parameters, l_s , on critical buckling load predicted by the Euler–Bernoulli and Timoshenko theories. The differences between critical buckling load obtained by RSGET, MCST and classical theory are significant when the length-to-thickness ratio, L/h , is low. The critical buckling load increases as the strain gradient length–scale parameter, l_s , increases.

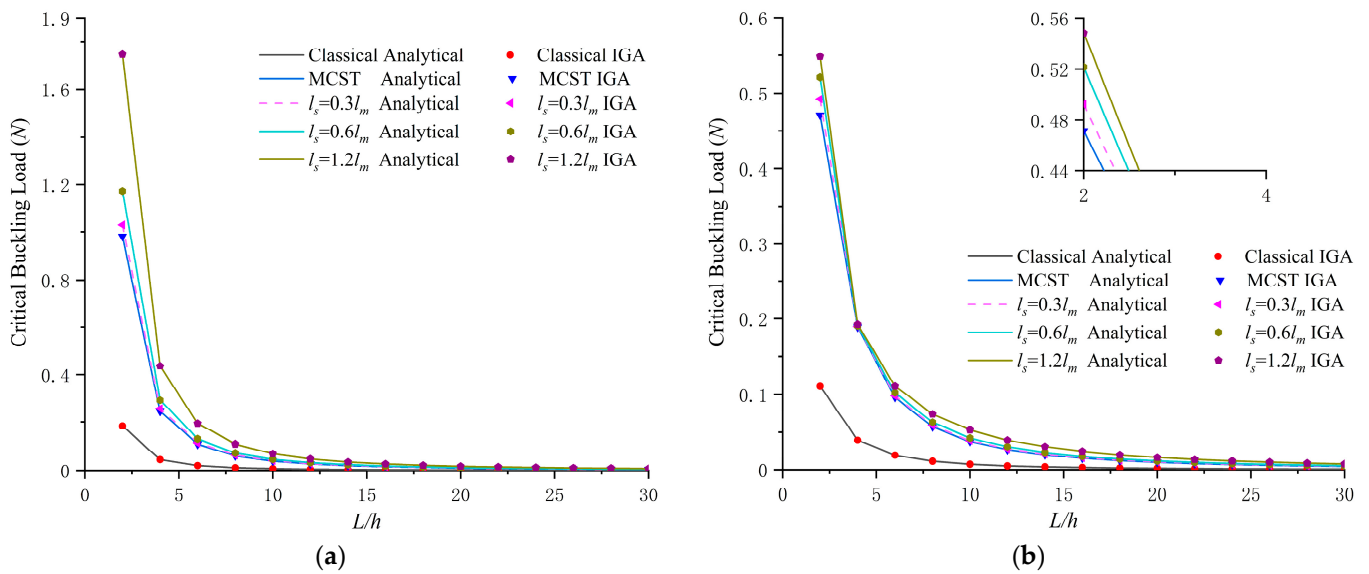


Figure 3. Critical buckling loads of the simply supported beam with different l_s . (a) Euler–Bernoulli; (b) Timoshenko.

Figure 4 presents the comparison of critical buckling loads obtained by EBT and TBT based on classical theory, MCST and RSGET with $l_s = 1.2l_m$. It can be clearly observed that the critical buckling load obtained by TBT is smaller than those obtained by EBT and the results obtained by TBT converge to EBT as the beam length increases. This matched with the general trends that suggest that the EBT is better suited to long beams or slender beams.

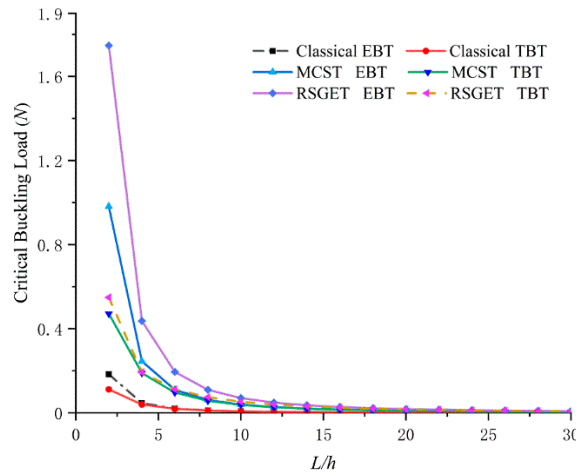
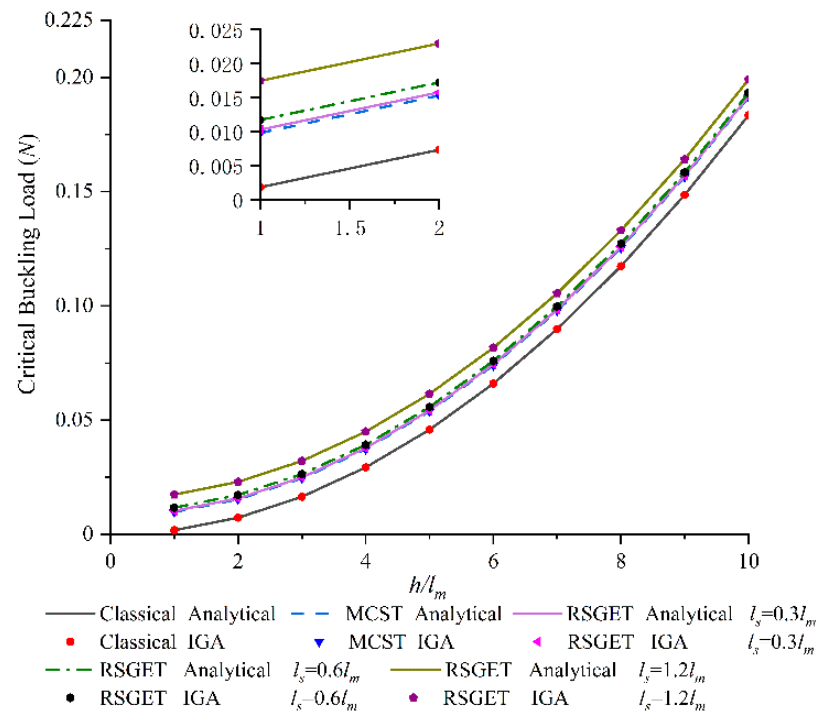
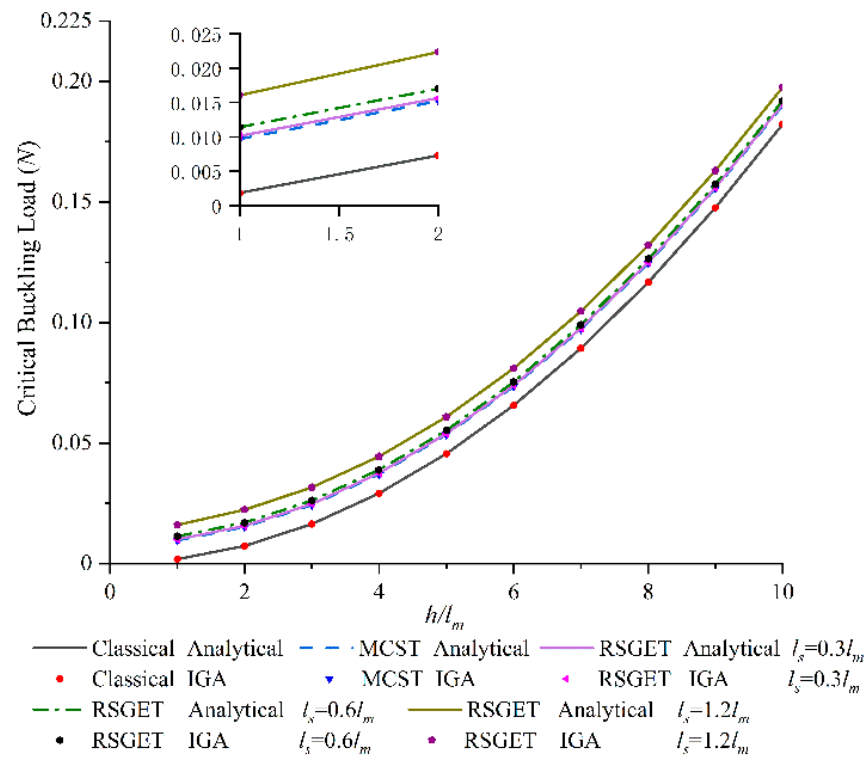


Figure 4. Comparison of critical buckling loads between EBT and TBT.

The influence of beam thickness on the critical buckling loads of EBT and TBT with different strain gradient length–scale parameters, l_s , are shown in Figure 5a,b, respectively. In this example, the geometries are $L = 20h$ and $b = 2h$ and the material–scale parameter is $l_m = 17.6 \mu\text{m}$. For both the Euler–Bernoulli and the Timoshenko beam problems, the IGA results matched very well with the analytical solutions. It shows that the critical buckling load increased as the beam thickness and strain gradient length–scale parameter, l_s , increased. On the other hand, it reveals that the size-dependent behavior can be described by the present IGA approach.



(a)



(b)

Figure 5. The critical buckling loads with different thickness and l_s . (a) Euler–Bernoulli; (b) Timoshenko.

Considering the former example, the comparison of critical buckling loads, obtained by EBT and TBT based on classical theory, and the MCST and RSGET with $l_s = 1.2l_m$ for different beam thickness, are shown in Figure 6. It shows that the difference between EBT and TBT is negligible for small values of beam thickness.

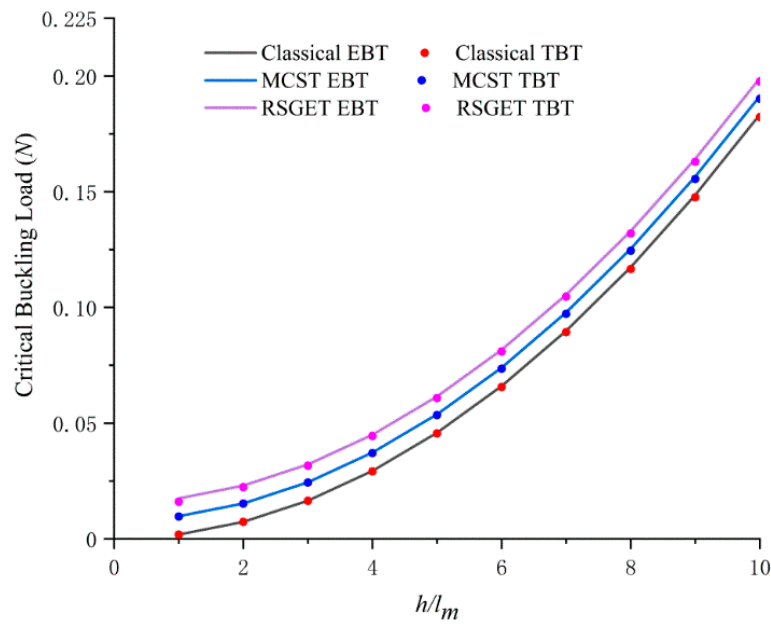


Figure 6. The critical buckling loads with different thickness.

In order to show the flexibility of the IGA approach, the effect of boundary conditions on the critical buckling load of EBT and TBT based on RSGET with $l_s = 1.2l_m$ are presented in Figure 7a,b. The geometry in here is defined by letting $L = 20h$ and $b = 2h$ and the material length–scale parameter is $l_m = 17.6 \mu\text{m}$. It is observed that the results obtained by clamped–clamped (c-c) boundary conditions are higher than those obtained by clamped–simply (c-s) and simply–simply (s-s) boundary conditions, respectively. Furthermore, the differences increased as the beam thickness increased. This is due to the stiffness changing with the boundary conditions, and led to the variation in critical buckling load, especially for thick beams.

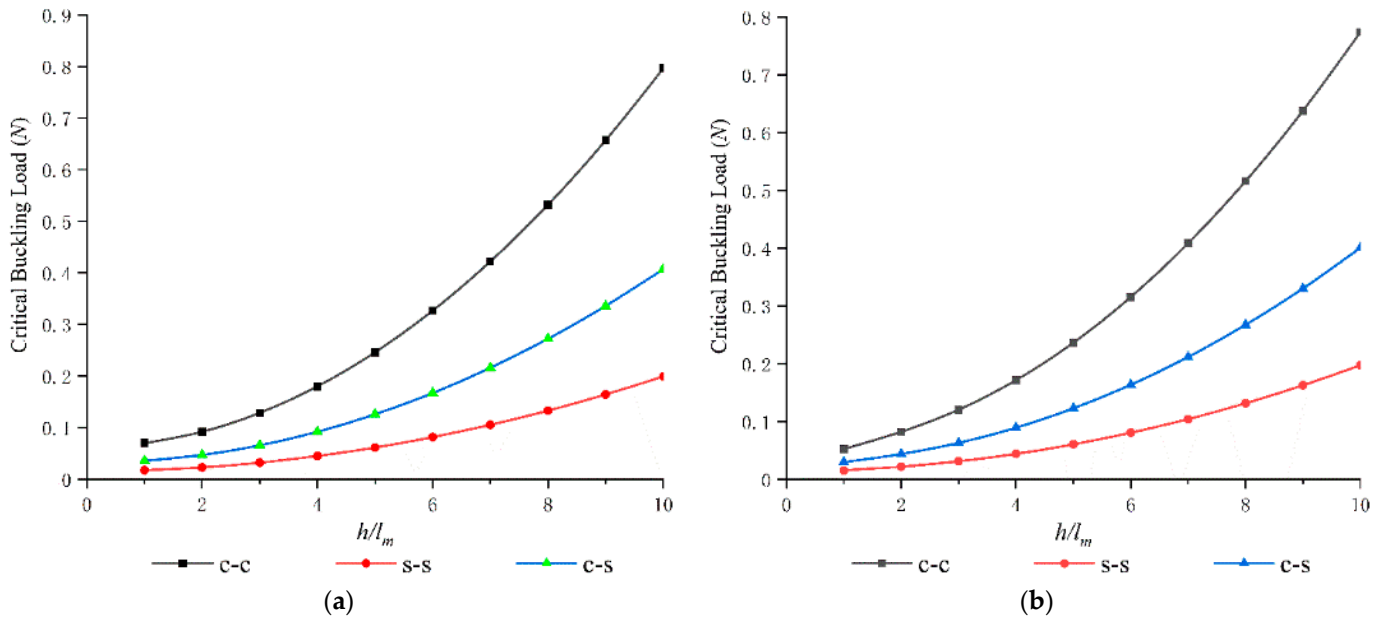


Figure 7. The critical buckling loads obtained by RSGT under different boundary conditions. (a) Euler–Bernoulli; (b) Timoshenko.

Finally, the influence of Poisson’s ratio on the critical buckling load of EBT and TBT with simply supported boundary condition are shown in Figure 8. The geometries are $b = 2h$ and $h = l_m = 17.6 \mu\text{m}$. It can be clearly seen that the effect of Poisson’s ratio increased as the L/h

decreased and the critical buckling load decreased as Poisson's ratio increased, which is in line with the general trends obtained in [41,71]. Therefore, a significant error may be produced by neglecting Poisson's ratio for thick beams.

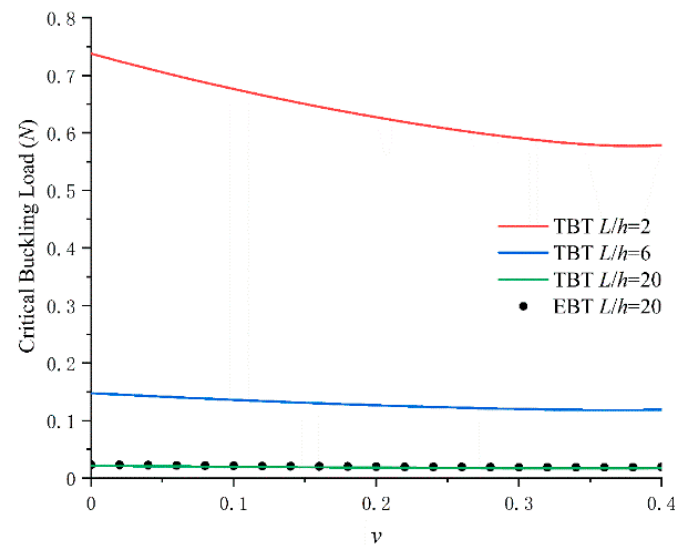


Figure 8. The critical buckling loads with different Poisson ratio.

6. Conclusions

In this work, the analytical method and an isogeometric analysis based on RSGET are presented for assessing the size-dependent buckling of Euler–Bernoulli and Timoshenko beams. The advantage of the present method is that it includes couple-stress and strain gradient effects with only one material parameter for each. Using the principle of minimum potential energy, the governing equations and boundary conditions of EBT and TBT can be derived. Moreover, the isogeometric analysis approach which satisfied the higher gradient requirements is proposed to solve the governing differential equations. The isogeometric analysis results are compared with exact solutions to validate its accuracy. The effects of the length–scale parameter, the length-to-thickness ratio, the beam thickness and the boundary conditions are studied. Moreover, the differences between the critical buckling loads obtained by the Euler–Bernoulli and Timoshenko beam theories shows that the Euler–Bernoulli theory is more suitable for slender beams.

Author Contributions: Conceptualization, G.Z.; methodology, S.Y.; validation, J.L.; formal analysis, S.Y., Z.X.; writing—original draft preparation, S.Y.; writing—review and editing, S.G.; supervision, S.G. All authors have read and agreed to the published version of the manuscript.

Funding: This work was funded by the National Natural Science Foundation of China (Grant No. 12002086, 52075465), the Hunan Provincial Natural Science Foundation of China (Grant No. 2021JJ30649), the Hunan Science Foundation for Distinguished Young Scholars (Grant No. 2019JJ20015), the Science and Technology innovation Program of Hunan Province (Grant No. 2020RC4038) and the Education Department of Hunan Province (Grant No. 20B565).

Conflicts of Interest: The authors declare no conflict of interest.

References

1. Younis, M.I.; Abdel-Rahman, E.M.; Nayfeh, A. A reduced-order model for electrically actuated microbeam-based MEMS. *J. Microelectromechanical Syst.* **2003**, *12*, 672–680. [[CrossRef](#)]
2. Wu, Z.Y.; Yang, H.; Li, X.X.; Wang, Y.L. Self-assembly and transfer of photoresist suspended over trenches for microbeam fabrication in MEMS. *J. Micromech. Microeng.* **2010**, *20*, 115014. [[CrossRef](#)]
3. Lee, H.-L.; Chang, W.-J. Sensitivity of V-shaped atomic force microscope cantilevers based on a modified couple stress theory. *Microelectron. Eng.* **2011**, *88*, 3214–3218. [[CrossRef](#)]
4. Lam, D.C.C.; Yang, F.; Chong, A.; Wang, J.; Tong, P. Experiments and theory in strain gradient elasticity. *J. Mech. Phys. Solids* **2003**, *51*, 1477–1508. [[CrossRef](#)]

5. McFarland, A.W.; Colton, J.S. Role of material microstructure in plate stiffness with relevance to micro cantilever sensors. *J. Micromech. Microeng.* **2005**, *15*, 1060–1067. [[CrossRef](#)]
6. Lourie, O.; Cox, D.M.; Wagner, H.D. Buckling and Collapse of Embedded Carbon Nanotubes. *Phys. Rev. Lett.* **1998**, *81*, 1638–1641. [[CrossRef](#)]
7. Waters, J.; Riester, L.; Jouzi, M.; Guduru, P.; Xu, J. Buckling instabilities in multiwalled carbon nanotubes under uniaxial compression. *Appl. Phys. Lett.* **2004**, *85*, 1787–1789. [[CrossRef](#)]
8. Mindlin, R.D. Micro-structure in linear elasticity. *Arch. Ration. Mech. Anal.* **1964**, *16*, 51–78. [[CrossRef](#)]
9. Mindlin, R.D.; Eshel, N.N. On first strain-gradient theories in linear elasticity. *Int. J. Solids Struct.* **1968**, *4*, 109–124. [[CrossRef](#)]
10. Eringen, A. Nonlocal polar elastic continua. *Int. J. Eng. Sci.* **1972**, *10*, 1–16. [[CrossRef](#)]
11. Eringen, A.C. On differential equations of nonlocal elasticity and solutions of screw dislocation and surface waves. *J. Appl. Phys.* **1983**, *54*, 4703–4710. [[CrossRef](#)]
12. Eringen, A.C. Theory of micropolar plates. *Z. Angew. Math Phys.* **1967**, *18*, 12–30. [[CrossRef](#)]
13. Mindlin, R.D.; Tiersten, H.F. Effects of couple-stresses in linear elasticity. *Arch. Ration. Mech. Anal.* **1962**, *11*, 415–448. [[CrossRef](#)]
14. Koiter, W.T. Couple stresses in the theory of elasticity: I and II. *Proc. K Ned. Akad. Wet B* **1964**, *67*, 17–44.
15. Toupin, R.A. Theories of elasticity with couple-stress. *Arch. Ration. Mech. Anal.* **1964**, *17*, 85–112. [[CrossRef](#)]
16. Polizzotto, C. A hierarchy of simplified constitutive models within isotropic strain gradient elasticity. *Eur. J. Mech.-A/Solids* **2017**, *61*, 92–109. [[CrossRef](#)]
17. Fleck, N.; Hutchinson, J.W. Strain Gradient plasticity. *Adv. Appl. Mech.* **1997**, *33*, 295–361.
18. Kong, S.; Zhou, S.; Nie, Z.; Wang, K. Static and dynamic analysis of microbeams based on strain gradient elasticity theory. *Int. J. Eng. Sci.* **2009**, *47*, 487–498. [[CrossRef](#)]
19. Wang, B.; Zhao, J.; Zhou, S. A microscale Timoshenko beam model based on strain gradient elasticity theory. *Eur. J. Mech. A/Solids* **2010**, *29*, 591–599. [[CrossRef](#)]
20. Akgöz, B.; Civalek, Ö. Strain gradient elasticity and modified couple stress models for buckling analysis of axially loaded micro-scaled beams. *Int. J. Eng. Sci.* **2011**, *49*, 1268–1280. [[CrossRef](#)]
21. Akgöz, B.; Civalek, Ö. Analysis of micro-sized beams for various boundary conditions based on the strain gradient elasticity theory. *Ingenieur-Archiv* **2012**, *82*, 423–443. [[CrossRef](#)]
22. Akgöz, B.; Civalek, Ö. Buckling analysis of functionally graded microbeams based on the strain gradient theory. *Acta Mech.* **2013**, *224*, 2185–2201. [[CrossRef](#)]
23. Ansari, R.; Gholami, R.; Sahmani, S. Free vibration analysis of size-dependent functionally graded microbeams based on the strain gradient Timoshenko beam theory. *Compos. Struct.* **2011**, *94*, 221–228. [[CrossRef](#)]
24. Reddy, J.N. Nonlocal theories for bending, buckling and vibration of beams. *Int. J. Eng. Sci.* **2007**, *45*, 288–307. [[CrossRef](#)]
25. Barretta, R.; Faghidian, S.A.; de Sciarra, F.M.; Vaccaro, M.S. Nonlocal strain gradient torsion of elastic beams: Variational formulation and constitutive boundary conditions. *Ingenieur-Archiv* **2020**, *90*, 691–706. [[CrossRef](#)]
26. Barretta, R.; Faghidian, S.A.; Marotti de Sciarra, F.; Penna, R.; Pinnola, F.P. On torsion of nonlocal Lam strain gradient FG elastic beams nonlocal elasticity theory. *Compos. Struct.* **2020**, *233*, 111550. [[CrossRef](#)]
27. Barretta, R.; Faghidian, S.A.; de Sciarra, F.M.; Pinnola, F.P. Timoshenko nonlocal strain gradient nanobeams: Variational consistency, exact solutions and carbon nanotube Young moduli. *Mech. Adv. Mater. Struct.* **2021**, *28*, 1523–1536. [[CrossRef](#)]
28. Thang, P.T.; Nguyen-Thoi, T.; Lee, J. Modeling and analysis of bi-directional functionally graded nanobeams based on nonlocal strain gradient theory. *Appl. Math. Comput.* **2021**, *407*, 126303. [[CrossRef](#)]
29. Jalaei, M.H.; Thai, H.T.; Civalek, Ö. On viscoelastic transient response of magnetically imperfect functionally graded nanobeams. *Int. J. Eng. Sci.* **2022**, *172*, 103629. [[CrossRef](#)]
30. Gao, X.-L.; Park, S. Variational formulation of a simplified strain gradient elasticity theory and its application to a pressurized thick-walled cylinder problem. *Int. J. Solids Struct.* **2007**, *44*, 7486–7499. [[CrossRef](#)]
31. Papargyri-Beskou, S.; Polyzos, D.; Beskos, D. Wave dispersion in gradient elastic solids and structures: A unified treatment. *Int. J. Solids Struct.* **2009**, *46*, 3751–3759. [[CrossRef](#)]
32. Gourgiotis, P.; Georgiadis, H. Plane-strain crack problems in microstructured solids governed by dipolar gradient elasticity. *J. Mech. Phys. Solids* **2009**, *57*, 1898–1920. [[CrossRef](#)]
33. Altan, B.; Aifantis, E. On Some Aspects in the Special Theory of Gradient Elasticity. *J. Mech. Behav. Mater.* **1997**, *8*, 231–282. [[CrossRef](#)]
34. Hong, J.; Zhang, G.; Wang, X.; Mi, C. A simplified strain gradient Kirchhoff rod model and its applications on microsprings and microcolumns. *J. Mech. Mater. Struct.* **2020**, *15*, 203–223. [[CrossRef](#)]
35. Liang, X.; Hu, S.; Shen, S. A new Bernoulli–Euler beam model based on a simplified strain gradient elasticity theory and its applications. *Compos. Struct.* **2014**, *111*, 317–323. [[CrossRef](#)]
36. Yang, F.; Chong, A.; Lam, D.; Tong, P. Couple stress based strain gradient theory for elasticity. *Int. J. Solids Struct.* **2002**, *39*, 2731–2743. [[CrossRef](#)]
37. Ebrahimi, F.; Barati, M.R.; Civalek, Ö. Application of Chebyshev–Ritz method for static stability and vibration analysis of nonlocal microstructure-dependent nanostructures. *Eng. Comput.* **2020**, *36*, 953–964.
38. Park, S.K.; Gao, X.-L. Variational formulation of a modified couple stress theory and its application to a simple shear problem. *Z. Angew. Math. Phys.* **2008**, *59*, 904–917. [[CrossRef](#)]

39. Park, S.K.; Gao, X.L. Bernoulli-Euler beam model based on a modified couple stress theory. *J. Micromech. Microeng.* **2006**, *16*, 2355–2359. [[CrossRef](#)]
40. Gao, X.-L.; Mahmoud, F.F. A new Bernoulli–Euler beam model incorporating microstructure and surface energy effects. *Z. Angew. Math. Phys.* **2014**, *65*, 393–404. [[CrossRef](#)]
41. Ma, H.; Gao, X.-L.; Reddy, J. A microstructure-dependent Timoshenko beam model based on a modified couple stress theory. *J. Mech. Phys. Solids* **2008**, *56*, 3379–3391. [[CrossRef](#)]
42. Gao, X.-L. A new Timoshenko beam model incorporating microstructure and surface energy effects. *Acta Mech.* **2015**, *226*, 457–474. [[CrossRef](#)]
43. Ma, H.M.; Gao, X.L.; Reddy, J.N. A non-classical Reddy–Levinson beam model based on a modified couple stress theory. *Int. J. Multiscale Comput. Eng.* **2010**, *8*, 167–180. [[CrossRef](#)]
44. Gao, X.-L.; Zhang, G.Y. A microstructure- and surface energy-dependent third-order shear deformation beam model. *Z. Angew. Math. Phys.* **2015**, *66*, 1871–1894. [[CrossRef](#)]
45. Hong, J.; Wang, S.; Zhang, G.; Mi, C. On the Bending and Vibration Analysis of Functionally Graded Magneto-Electro-Elastic Timoshenko Microbeams. *Crystals* **2021**, *11*, 1206. [[CrossRef](#)]
46. Hong, J.; Wang, S.; Qiu, X.; Zhang, G. Bending and Wave Propagation Analysis of Magneto-Electro-Elastic Functionally Graded Porous Microbeams. *Crystals* **2022**, *12*, 732. [[CrossRef](#)]
47. Zhang, G.; Gao, X.-L. A new Bernoulli–Euler beam model based on a reformulated strain gradient elasticity theory. *Math. Mech. Solids* **2020**, *25*, 630–643. [[CrossRef](#)]
48. Hong, J.; Wang, S.; Zhang, G.; Mi, C. Bending, Buckling and Vibration Analysis of Complete Microstructure-Dependent Functionally Graded Material Microbeams. *Int. J. Appl. Mech.* **2021**, *13*, 2150057. [[CrossRef](#)]
49. Amanatidou, E.; Aravas, N. Mixed finite element formulations of strain-gradient elasticity problems. *Comput. Methods Appl. Mech. Eng.* **2002**, *191*, 1723–1751. [[CrossRef](#)]
50. Zhang, B.; He, Y.; Liu, D.; Gan, Z.; Shen, L. A non-classical Mindlin plate finite element based on a modified couple stress theory. *Eur. J. Mech.-A/Solids* **2013**, *42*, 63–80. [[CrossRef](#)]
51. Phunpeng, V.; Baiz, P.M. Mixed finite element formulations for strain-gradient elasticity problems using the FEniCS environment. *Finite Elem. Anal. Des.* **2015**, *96*, 23–40. [[CrossRef](#)]
52. Pinnola, F.P.; Vaccaro, M.S.; Barretta, R.; de Sciarra, F.M. Finite element method for stress-driven nonlocal beams. *Eng. Anal. Bound. Elements* **2022**, *134*, 22–34. [[CrossRef](#)]
53. Hughes, T.J.; Cottrell, J.A.; Bazilevs, Y. Isogeometric analysis: CAD, finite elements, NURBS, exact geometry and mesh refinement. *Comput. Meth. Appl. Mech. Eng.* **2005**, *194*, 4135–4195. [[CrossRef](#)]
54. Nguyen, N.T.; Hui, D.; Lee, J.; Nguyen-Xuan, H. An efficient computational approach for size-dependent analysis of functionally graded nanoplates. *Comput. Meth. Appl. Mech. Eng.* **2015**, *297*, 191–218. [[CrossRef](#)]
55. Ansari, R.; Norouzzadeh, A. Nonlocal and surface effects on the buckling behavior of functionally graded nanoplates: An isogeometric analysis. *Phys. E Low-Dimens. Syst. Nanostructures* **2016**, *84*, 84–97. [[CrossRef](#)]
56. Phung-Van, P.; Thai, C.H.; Nguyen-Xuan, H.; Wahab, M.A. Porosity-dependent nonlinear transient responses of functionally graded nanoplates using isogeometric analysis. *Compos. Part B: Eng.* **2019**, *164*, 215–225. [[CrossRef](#)]
57. Phung-Van, P.; Thai, C.H.; Wahab, M.A.; Nguyen-Xuan, H. Optimal design of FG sandwich nanoplates using size-dependent isogeometric analysis. *Mech. Mater.* **2020**, *142*, 103277. [[CrossRef](#)]
58. Phung-Van, P.; Ferreira, A.J.M.; Thai, C.H. Computational optimization for porosity-dependent isogeometric analysis of functionally graded sandwich nanoplates. *Compos. Struct.* **2020**, *239*, 112029. [[CrossRef](#)]
59. Nguyen, H.X.; Atroshchenko, E.; Nguyen-Xuan, H.; Vo, T.P. Geometrically nonlinear isogeometric analysis of functionally graded microplates with the modified couple stress theory. *Comput. Struct.* **2017**, *193*, 110–127. [[CrossRef](#)]
60. Liu, S.; Yu, T.; Van Lich, L.; Yin, S.; Bui, T.Q. Size and surface effects on mechanical behavior of thin nanoplates incorporating microstructures using isogeometric analysis. *Comput. Struct.* **2019**, *212*, 173–187. [[CrossRef](#)]
61. Thanh, C.-L.; Phung-Van, P.; Thai, C.H.; Nguyen-Xuan, H.; Wahab, M.A. Isogeometric analysis of functionally graded carbon nanotube reinforced composite nanoplates using modified couple stress theory. *Compos. Struct.* **2018**, *184*, 633–649. [[CrossRef](#)]
62. Farzam, A.; Hassani, B. Thermal and mechanical buckling analysis of FG carbon nanotube reinforced composite plates using modified couple stress theory and isogeometric approach. *Compos. Struct.* **2018**, *206*, 774–790. [[CrossRef](#)]
63. Thai, S.; Thai, H.-T.; Vo, T.P.; Patel, V.I. Size-dependant behaviour of functionally graded microplates based on the modified strain gradient elasticity theory and isogeometric analysis. *Comput. Struct.* **2017**, *190*, 219–241. [[CrossRef](#)]
64. Yin, S.; Deng, Y.; Zhang, G.; Yu, T.; Gu, S. A new isogeometric Timoshenko beam model incorporating microstructures and surface energy effects. *Math. Mech. Solids* **2020**, *25*, 2005–2022. [[CrossRef](#)]
65. Yin, S.; Deng, Y.; Yu, T.; Gu, S.; Zhang, G. Isogeometric analysis for non-classical Bernoulli-Euler beam model incorporating microstructure and surface energy effects. *Appl. Math. Model.* **2021**, *89*, 470–485. [[CrossRef](#)]
66. Yin, S.; Xiao, Z.; Deng, Y.; Zhang, G.; Liu, J.; Gu, S. Isogeometric analysis of size-dependent Bernoulli–Euler beam based on a reformulated strain gradient elasticity theory. *Comput. Struct.* **2021**, *253*, 106577. [[CrossRef](#)]
67. Yin, S.H.; Xiao, Z.B.; Liu, J.G.; Xia, Z.X.; Gu, S.T. Variational formulations and isogeometric analysis of Timoshenko–Ehrenfest microbeam using a reformulated strain gradient elasticity theory. *Crystals* **2022**, *12*, 752. [[CrossRef](#)]

68. Phung-Van, P.; Ferreira, A.; Nguyen-Xuan, H.; Thai, C.H. Scale-dependent nonlocal strain gradient isogeometric analysis of metal foam nanoscale plates with various porosity distributions. *Compos. Struct.* **2021**, *268*, 113949. [[CrossRef](#)]
69. Shaat, M. A reduced micromorphic model for multiscale materials and its applications in wave propagation. *Compos. Struct.* **2018**, *201*, 446–454. [[CrossRef](#)]
70. Zhang, G.; Gao, X.-L.; Zheng, C.; Mi, C. A non-classical Bernoulli-Euler beam model based on a simplified micromorphic elasticity theory. *Mech. Mater.* **2021**, *161*, 103967. [[CrossRef](#)]
71. Mohammad-Abadi, M.; Daneshmehr, A. Size dependent buckling analysis of microbeams based on modified couple stress theory with high order theories and general boundary conditions. *Int. J. Eng. Sci.* **2014**, *74*, 1–14. [[CrossRef](#)]
72. Qu, Y.; Zhang, G.; Fan, Y.; Jin, F. A non-classical theory of elastic dielectrics incorporating couple stress and quadrupole effects: Part I—Reconsideration of curvature-based flexoelectricity theory. *Math. Mech. Solids* **2021**, *26*, 1647–1659. [[CrossRef](#)]
73. Gao, X.-L.; Mall, S. Variational solution for a cracked mosaic model of woven fabric composites. *Int. J. Solids Struct.* **2001**, *38*, 855–874. [[CrossRef](#)]